phys. stat. sol. (a) **202**, No. 5, 732–738 (2005) / **DOI** 10.1002/pssa.200461364

White X-ray microbeam analysis of strain and crystallographic tilt in GaN layers grown by maskless pendeoepitaxy

R. I. Barabash[*, 1], **G. E. Ice**[1], **W. Liu**[1], **S. Einfeldt**[2], **D. Hommel**[2], **A. M. Roskowski**[3], and **R. F. Davis**[3]

[1] Metals and Ceramics Div., Oak Ridge National Laboratory, Oak Ridge, TN 37831, USA
[2] Institute of Solid State Physics, University of Bremen, 28334 Bremen, Germany
[3] Department of Materials Science and Engineering, North Carolina State University, Raleigh, NC 27695, USA

Received 9 July 2004, revised 12 November 2004, accepted 22 February 2005
Published online 4 April 2005

PACS 61.10.Nz, 61.72.Ff, 68.35.Ct, 68.35.Gy, 68.55.Jk, 81.15.Gh

We describe X-ray and finite element analysis of dislocations, strain and crystallographic tilt in uncoalesced GaN layers grown by maskless pendeoepitaxy. The experimental results reveal that the GaN wings are tilted upward at room temperature. The distribution of strain and tilt depends on the width-to-height ratio of the GaN column. As the width-to-height ratio increases the wing tilt increases and changes more abruptly at the column/wing interface. Broadening of the GaN Laue reflections is more pronounced in the column region then in the wing region; this is in line with the inhomogeneity of both the strain and the defect density. A split in the Laue reflections from GaN films at the column/wing interface indicates the development of a low-angle tilt boundary for samples with a large width-to-height ratio of the column. Spacing between the dislocations in the tilt boundary at the column/wing interface for GaN grown with *maskless* pendeoepitaxy is an order of magnitude larger than the dislocation spacing observed for *masked* lateral epitaxial growth.

© 2005 WILEY-VCH Verlag GmbH & Co. KGaA, Weinheim

1 Introduction

When GaN films are grown on available substrates like sapphire or SiC, they are found to contain a high density of threading dislocations (10^{10} cm^{-2}) due to lattice mismatch and due to orientational differences between coalescing islands [1, 2]. Dislocations are known to impair the performance of GaN-based light emitting devices; they cause nonradiative recombination (i.e. influence luminescence efficiency) and decrease carrier mobility. Dislocations also act as parasitic current paths in p–n junctions and shorten the lifetime of laser-diodes. These undesirable traits have stimulated the development of growing techniques intended to prevent the formation of dislocations in the GaN layers.

Lateral epitaxial overgrowth (LEO) techniques such as pendeoepitaxy [3–5] have recently been shown to greatly reduce the density of threading dislocations. In the pendeoepitaxy process, GaN wings are grown from the sides of GaN columns (Fig. 1a). The top of the column may or may not be covered with a mask (masked or maskless pendeoepitaxy) to inhibit GaN growth. When the LEO process is continued until the overgrowth of a mask, threading dislocations are observed to form a grain boundary along the edge of the mask [6, 7]. This grain boundary is related to the crystallographic tilt of the later-

[*] Corresponding author: e-mail: barabashr@ornl.gov

© 2005 WILEY-VCH Verlag GmbH & Co. KGaA, Weinheim

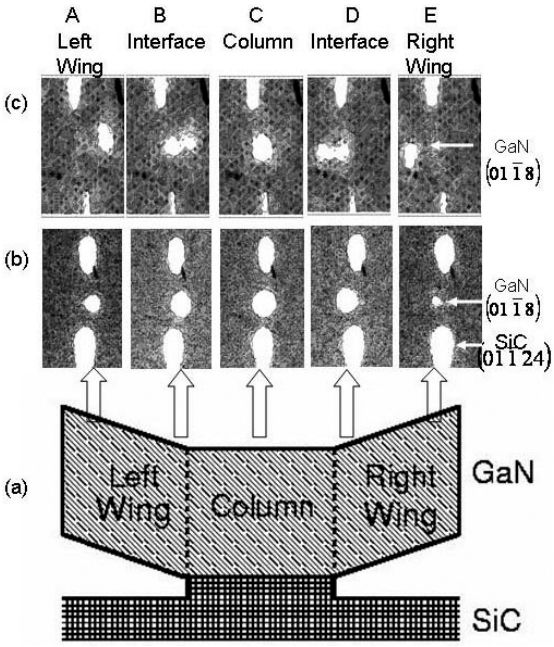

Fig. 1 Scheme of the sample geometry (a) together with a series of Laue images showing the (01$\bar{1}$8) GaN reflection in the center. The Laue images for sample 2 (b) and 1 (c) correspond to different locations of the probing beam across the stripe: (A) center of the left wing; (B) left wing/column interface; (C) center of the column; (D) column/right wing interface; (E) center of the right wing.

ally growing wings which usually accompanies all LEO techniques. On the other hand, in the case of maskless pendeoepitaxy [8–10] for which the growth starts from the sidewalls and *simultaneously* from the surface of unmasked GaN columns, the wing tilt depends on the *c*-axis strain in the columns [10]. The GaN layers grown with maskeless pendeoepitaxy are thought to be different from those grown with mask.

Curiously, it is not possible to explain all experimental data by the elastic relief of stress in LEO structures. For example, differences between experiment and elasticity theory were found for the correlations between in-plane strains, dimensions of the column and wing tilt. For both masked and maskless pendeoepitaxy, point and extended defects generated in the GaN during overgrowth are assumed to play as an important role in the formation of strains and wing tilt as does the mismatch in the coefficients of thermal expansion between GaN and the substrate. Despite extensive characterization, the basic structure of LEO films including such critical information as the direction of the wing tilt remains controversial. The application of powerful X-ray white beam microdiffraction (WBMD) to this important problem together with finite element (FE) simulation and high resolution X-ray diffraction (HRXRD) has enabled us to provide detailed new information on the structure of these materials.

2 Experimentals

GaN stripes along [1$\bar{1}$00] direction having a rectangular cross section were etched from 1 μm thick GaN single crystal layers grown by metalorganic vapor phase epitaxy on 0.1 μm thick AlN buffer layer deposited on 6H–SiC (0001) substrate. The subsequent overgrowth process was stopped before the wings coalesced. A schematic of the stripe geometry is shown in Fig. 1a. Details of the growth process were reported separately [9, 11]. Two samples with different GaN stripe geometries were analyzed. The GaN thickness, the column width and the wing width were 1.46 μm, 3.80 μm, and 0.98 μm for sample 1 and 3.53 μm, 3.46 μm and 1.74 μm for sample 2.

Data collection with WBMD has been carried out at the beamline ID-34-E at the Advanced Photon Source, Argonne IL. This method uses a modified Laue diffraction technique. It allows for true 3D mapping of crystalline phase, orientation, elastic strain and plastic deformation with 0.5 μm spatial resolution [12]. As the polychromatic beam penetrates the sample, it produces a Laue pattern in each volume elementy (VOXEL) that it intercepts. The superimposed Laue patterns are detected by an X-ray sensitive CCD positioned at 90° to the incident beam.

© 2005 WILEY-VCH Verlag GmbH & Co. KGaA, Weinheim

WBMD for samples with minimal deformation has an angular resolution of <0.01°. This makes it possible to quantitatively determine the GaN tilt as a function of distance from the center of the column. Further details on the experimental setup and the data collection can be found elsewhere [12–14]. HRXRD measurements were performed using a Philips X'Pert MRD diffractometer equipped with a fourbounce Ge(220) monochromator with the wavelength 1.540598 Å and a three bounce Ge (220) analyzer. Two-dimensional FE simulations were conducted as described in Ref. [10].

3 Results and discussion

The white microbeam was scanned perpendicular to the stripe axis, and Laue patterns were recorded at 1000 different points with a spacing of 0.25 μm. Several (usually 10–20) parallel line scans were recorded to obtain a 2D map of the sample. Due to the small size of the microbeam it was possible to obtain separate images from different locations on the column and the wings. Because the high-energy X-ray beam passes through the GaN and the AlN layers, the SiC substrate contributes to the observed Laue patterns. The reflections originating from the SiC are superimposed on those from the GaN for all the WBMD images. A typical series of WBMD images at different locations along the line scan perpendicular to the stripe direction are shown in Figs. 1b, c for samples 1 and 2. The Cartesian reference frame is set such that the *y*-axis coincides with the $[1\bar{1}00]$ direction of the GaN stripe. The *x*-axis is perpendicular to the stripe in the plane of the GaN film in the $[11\bar{2}0]$ direction. In this coordinate system the beam is incident to the surface at ~45° with components $\left(0, \frac{1}{\sqrt{2}}, \frac{-1}{\sqrt{2}}\right)$.

A typical line scan moves the sample under the beam in the *x*-axis which exposes different parts of the column, wing and substrate structure. Two Laue reflections belonging to the SiC and one GaN reflection located at the vertical zone line with the zone axis running along the *x*-direction are shown at Figs. 1b, c. The SiC reflections do not change position with sample translation. The SiC Laue reflections were used as a reference to determine the position of the GaN $(01\bar{1}8)$ Laue reflection. When the probing spot is moved along the positive *x*-axis and first hits the left wing, the GaN reflection appears at the right side of the SiC reflections, as shown in images A of Figs. 1b, c. As the probe spot is moved across the wing to the wing/column interface the split GaN reflections can be observed for sample 1 (image B of Fig. 1c) – one from the wing and one from the column. When the probe is in the center of the column, the GaN reflections are aligned with the SiC reflections for both samples, as shown (C of Figs. 1b and c). With further displacement towards the right wing the GaN reflections appear to the left of the SiC reflections (compare image D and E of Figs. 1b and c). The shift of the GaN reflections along with the geometry of the structure (Fig. 1a), clearly indicates that the wings are tilted upward.

An upward-tilt of the wings is also predicted by FE simulations as shown in Fig. 2. For the calculations it was assumed that the GaN is under biaxial tensile stress in the *c*-plane due to the mismatch in thermal expansion coefficients between the GaN layer and the SiC substrate. The stress along the *x*-direction is increasingly relieved towards the GaN surface as the uncoalesced GaN layer contracts laterally. The inhomogeneous stress relief results in the inclination of the stripe/wing interface plane and, consequently, in the upward-tilt of the wings [10]. FE simulations of displacements in the *z*-directions (Fig. 2) for the geometry corresponding to both samples also show that the wing tilt tends to increase with increasing width-to-height ratio of the column.

This is in agreement with the experimental WBMD data; sample 1 has a width-to-height ratio of the column of 2.60 and a wing tilt of 0.16°, whereas the corresponding numbers for sample 2 are 0.98 and 0.08°, respectively. Moreover, the WBMD data presented in Fig. 3 demonstrates that the crystallographic tilt changes quite abruptly at the column/wing interface for sample 1. In sample 2, however, this change is more gradual, and extends over the whole column between the right and left wing.

This finding is also in good agreement with the results of HRXRD. Figure 4 collects reciprocal space maps (RSMs) of the (0002) GaN reflection obtained by HRXRD for both samples with the diffraction plane being perpendicular to the stripes. Three peaks can be found which correspond to the left wings,

© 2005 WILEY-VCH Verlag GmbH & Co. KGaA, Weinheim

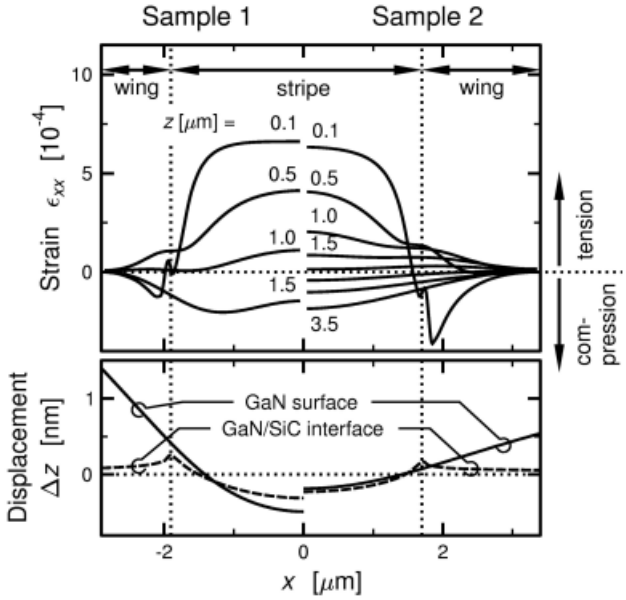

Fig. 2 Profiles of the normal strain in GaN layers along the x-axis at different depth (top) and displacement along the z-axis (bottom) as determined from FE simulations for sample 1 (left side) and 2 (right side), respectively. The height $z = 0$ corresponds to the GaN/SiC interface.

the columns and the right wings, respectively. As RSMs are practically symmetric relative to the central peak of the column, only half of RSMs for both samples are shown at Fig. 4.

The separation of the peaks along the q_x-axis reflects the different orientation of the c-axis of the three regions, i.e. the wing tilt. The corresponding values extracted from these measurements are 0.159° and 0.085° for sample 1 and 2, respectively. It is worth noting that in HRXRD the spot size of the X-ray beam is large (~0.5 mm), i.e. the RSM gives the averaged information over about 50 of stripes. In contrast, WBMD provides very local information and enables us to follow the change of the tilt in different locations across the stripe. The good agreement between the HRXRD and the WBMD results suggests that the wing tilt is quite homogeneous across the samples.

In Laue diffraction, the incident beam and scattered beam directions define a radial line in reciprocal space. The position along this line is determined by the wavelength of the scattered radiation. For example reciprocal lattice points (00h), (002h), (003h) etc. are scattered towards the same pixel on a CCD but lie at different positions radially in reciprocal space. To analyze the white beam intensity distribution we introduce a special misorientation vector $\boldsymbol{m}$ near a Bragg reflection. The misorientation vector $\boldsymbol{m}$ gives

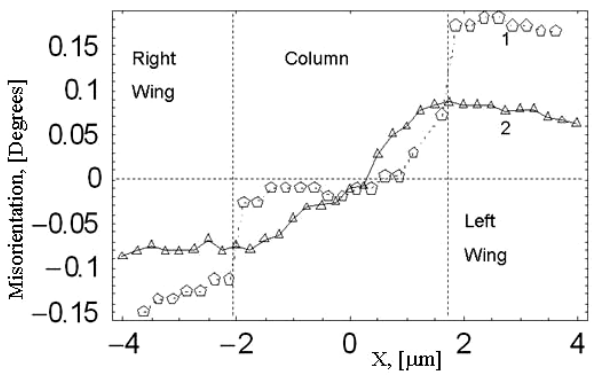

Fig. 3 Relative crystallographic orientation of the GaN c-axis across the stripe with distance from the column center as determined from WBMD analysis for sample 1 and 2.

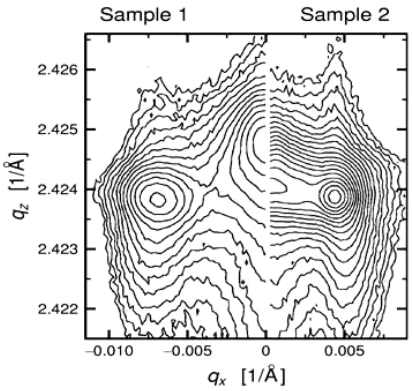

Fig. 4 HRXRD reciprocal space maps of the GaN (0002) reflection for sample 1 (left) and sample 2 (right).

© 2005 WILEY-VCH Verlag GmbH & Co. KGaA, Weinheim

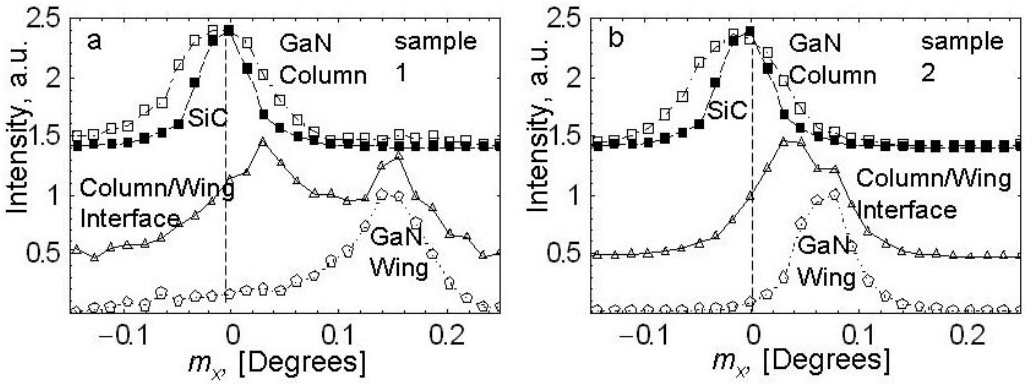

Fig. 5 WBMD line scans through the GaN $(01\bar{1}8)$ Laue reflection as a function of m_x for column, wing and column/wing interface for sample 1 (a) and sample 2 (b). Profile of the line scan from SiC is also shown for a comparison.

the difference between the unit vector parallel to Bragg reflection (hkl), $\hat{\boldsymbol{k}}_{hkl}$ and an arbitrary direction in its vicinity $\hat{\boldsymbol{k}}$; $\hat{\boldsymbol{m}} = \hat{\boldsymbol{k}} - \hat{\boldsymbol{k}}_{hkl}$. All results of WBMD are shown as a function of the above misorientation vector $\boldsymbol{m}$ in the direction $[11\bar{2}0]$ perpendicular to stripe.

The broadening of the GaN Laue reflections at different locations of the wings and column can be analyzed at corresponding positions along the WBDM line scans, as shown in Fig. 5. Comparing sample 1 and 2, the broadening is generally more pronounced for sample 1, i.e. the sample with the larger width-to-height ratio of the GaN column. Moreover, the reflection corresponding to the column is more broadened than the reflection corresponding to the wing (Fig. 5a). The ratio of the corresponding peak widths is about $1.2 \pm 5\%$ and $1.9 \pm 10\%$ for sample 1 and 2, respectively. A similar result is obtained from the HRXRD (0002) rocking curves. The ratio of the peak widths for the column and wing is unity and 3 for sample 1 and 2, respectively. For sample 1 the linescans in Fig. 5a show that the GaN reflection is particularly broadened at the column/wing interface where it splits into two distinct peaks. It should be noted that it is this sample for which the wing tilt changes abruptly at this interface, as was shown in Fig. 3. The splitting profile shows clearly resolved peaks, which indicates that wings and column have their own well-defined orientation. SEM analysis [10] of the sample 1 shows no signature of cracks close to the column/wing interface and/or parallel to it at the lower surface of the wing. This indicates that a small angle tilt boundary has formed at the column/wing interface in sample 1. For sample 2 (with smaller width-to-height ratio of the GaN column), however, this seems not to be the case. Figure 5b shows that the crystallographic orientation gradually changes across the stripe for sample 2 as was already discussed (Fig. 3). Due to the orientation spread in the column the width of the column peak obtained by HRXRD for sample 2 is much higher than the broadening measured by WBMD at each local position within the column. The resolved splitting at the column/wing interface for the sample 2 is several times less than for sample 1.

It is known [9], that GaN layers mimic the domain tilt of the substrate when grown on 6H–SiC (0001) wafers. Therefore, the profiles of the Laue reflections of GaN columns and SiC in m_x direction across the stripe are plotted together in Fig. 5. The width of the SiC Laue reflection remains the same at all locations. The GaN Laue reflections in the region of the column are always broader than the SiC reflections. This indicates that the broadening of the GaN reflection in this region is not due to imperfections of the substrate but arises mainly due to defects such as threading dislocations and to an inhomogeneous crystallographic orientation within the column.

In comparison to the column, the width of the GaN reflections from the wing regions are much smaller for both samples, and are about the same as the widths of the SiC reflections (although for sample 1 the wing reflection is somewhat broader than for sample 2). This confirms that the density of defects and the inhomogeneity of the strain are reduced in the wings as compared to the column.

© 2005 WILEY-VCH Verlag GmbH & Co. KGaA, Weinheim

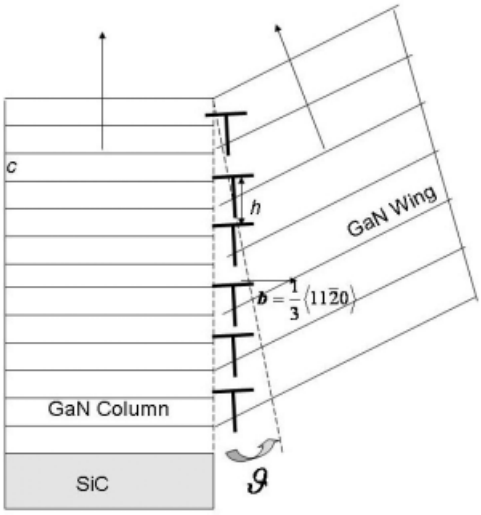

Fig. 6 Schematic of the dislocation arrangement in the tilt small angle boundary at the column/wing interface.

The dislocation arrangement at the column/wing interface can be modeled based on the results of WBMD (Fig. 6). The WBMD results indicate that the column/wing interface forms a tilt boundary; the rotation axis is parallel to the plane of the boundary and coincides with the experimental *y*-axis which is parallel to the $[1\bar{1}00]$ direction. The tilt is probably accommodated by edge dislocations with Burgers vector along $\frac{1}{3}\langle 11\bar{2}0\rangle$ direction. The upward wing tilt indicates that the boundary dislocations introduce additional half planes in lower part of the GaN column/wing interface. The observed tilt occurs due to the accumulated dislocations along the [0001] direction.

From the splitting of the GaN Laue spots, the misorientation between the column and wings at their interface was quantified. Using the measured misorientation at the column/wing interface, the spacing between dislocations in the boundary can be derived using the Burgers relation for a small angle tilt boundary: $\vartheta = b/h$. Here ϑ is the measured tilt angle at the interface, b is the Burgers vector modulus and h is the spacing between dislocations in the boundary. The tilt angle at the column/wing interface was always smaller then the total tilt between wing and column (especially for the sample 2). This means that thermal stresses were only partially relieved by the interface tilt boundary and some elastic strain remained. For the measured tilt angle at the interface between column and wing Laue spots of $\vartheta = \vartheta_1 = 0.12°$ for sample 1 and $\vartheta = \vartheta_2 = 0.04°$for sample 2 and for the $b = \frac{1}{3}\langle 11\bar{2}0\rangle$ we obtain the distance between dislocations in the tilt interface boundary $h_1 = 98c$ for sample 1 and $h_2 = 294c$ for sample 2. Here c is the interatomic distance along the *z*-axis of the GaN. For a GaN layer thickness of 1.46 μm or 3.53 μm in the sample 1 or 2 this amounts to 29 dislocations in the interface tilt boundary for sample 1 versus 23 dislocations for sample 2. Usually near the surface the distance between the boundary dislocations becomes less, as shown at the Fig. 6. The dislocation spacing in the boundary for GaN layers grown with maskless pendeoepitaxy even for the sample 1 is more then seven times larger than for GaN layers grown with mask [6].

4 Concluding remarks

X-ray WBMD experiments have shown that the crystallographic tilt of the wings in GaN layers grown on SiC substrates by maskless pendeoepitaxy is upward. This is consistent with FE simulations which assume the elastic relief of thermally induced tensile stress in the GaN. The distribution of the tilt across the stripe depends on the width-to-height ratio of the column and on the thickness of the overgrown GaN layer, respectively, which is in qualitative agreement with the FE simulations. For small width-to-height ratios the tilt is small, and it changes gradually in the region of the column. For larger width-to-height ratios the tilt is higher, and it changes abruptly at the wing/column interface. The evaluation of the local broadening of the reflections and their intensity profiles revealed that the density of defects was reduced

© 2005 WILEY-VCH Verlag GmbH & Co. KGaA, Weinheim

and/or the strain was homogenized in the wings as compared to the column. Moreover, a low-angle tilt boundary is formed at the column/wing interface in samples with larger width-to-height ratio of the GaN column. The estimated dislocation spacing at the column/wing interface is approximately three times smaller in the sample 1 than in sample 2.

Acknowledgements The research was supported in part by the U.S. Department of Energy, Division of Materials Sciences and Engineering through a contract with the Oak Ridge National Laboratory. Oak Ridge National Laboratory (ORNL) is operated by UT-Battelle, LLC, for the U.S. Department of Energy under contract DE-AC05-00OR22725. The research at NCSU was sponsored by the Office of Naval Research via contract N00014-98-1-0654 (Harry Dietrich, monitor). Measurements were performed on the Unicat beamline 34-ID at the Advanced Photon Source. The UNICAT facility at the Advanced Photon Source (APS) is supported by the U.S. DOE under Award No. DEFG02-91ER45439, through the Frederick Seitz Materials Research Laboratory at the University of Illinois at Urbana-Champaign and the Oak Ridge National Laboratory (U.S. DOE contract DE-AC05-00OR22725 with UT-Battelle LLC). The APS is supported by the U.S. DOE, Basic Energy Sciences, Office of Science under contract No. W-31-109-ENG-38.

The submitted manuscript has been authored by a contractor of the U.S. Government under contract No. DE-AC05-00OR22725. Accordingly, the U.S. Government retains a nonexclusive, royalty-free license to publish or reproduce the published form of this contribution, or allow others to do so, for U.S. Government purposes.

References

[1] S. D. Lester, F. A. Ponce, M. G. Craford, and D. A. Steigerwald, Appl. Phys. Lett. **66**, 1249 (1995).
[2] T. Metzger, R. Hopler, and E. Born, Philos. Mag. A **77**, 1013 (1998).
[3] S. Einfeldt, Z. J. Reitmeier, and R. F. Davis, J. Cryst. Growth **253**, 129 (2003).
[4] O.-H. Nam, M. D. Bremser, T. S. Tsvetanka, and R. F. Davis, Appl. Phys. Lett. **71**, 2638 (1997).
[5] K. Linthicum, T. Gehrke, D. Thomson, E. Carlson, P. Rajagopal, T. Smith, D. Batchelor, and R. Davis, Appl. Phys. Lett. **75**, 196 (1999).
[6] A. Sakai, H. Sunakawa, and A. Usui, Appl. Phys. Lett. **73**, 481 (1998).
[7] H. Marchand, X. H. Wu, J. P. Ibbetson, P. T. Fini, P. Kozodoy, S. Keller, J. S. Speck, S. P. DenBaars, and U. K. Mishra, Appl. Phys. Lett. **73**, 747 (1998).
[8] T. S. Zheleva, S. A. Smith, D. B. Thomson, T. Gehrke, K. J. Linthicum, P. Rajagopal, E. Carlson, W. Ashmawi, and R. F. Davis, MRS Internet J. Nitride Semicond. Res. **4S1**, G3.38 (1999).
[9] A. M. Roskowski, P. Q. Miraglia, E. A. Preble, S. Einfeldt, T. Stiles, R. F. Davis, J. Schuck, R. Grober, and U. Schwarz, phys. stat. sol. (a) **188**, 729 (2001).
[10] S. Einfeldt, A. M. Roskowski, E. A. Preble, and R. F. Davis, Appl. Phys. Lett. **80**, 953 (2002).
[11] R. F. Davis, S. Einfeldt, E. A. Preble, A. M. Roskowski, Z. J. Reitmeier, and P. Q. Miraglia, Acta Mater. **51**, 5961 (2003).
[12] B. C. Larson, Wenge Yang, G. E. Ice, J. D. Budai, and J. Z. Tischler, Nature **415**, 887 (2002).
[13] R. Barabash, G. Ice, B. Larson, G. Pharr, K. Chung, and W. Yang, Appl. Phys. Lett. **79**, 749 (2001).
[14] R. Barabash, G. Ice, and F. Walker, J. Appl. Phys. **93**, 1457 (2003).

© 2005 WILEY-VCH Verlag GmbH & Co. KGaA, Weinheim